Engineered Science
DOI: https://dx.doi.org/10.30919/es963

Analytical Solution of Seismic Responses of Multi-Storey Building Structures Controlled by Tuned Mass-Damper-Inerter (TMDI)

Ayman Abd-Elhamed[1, 2,*] and Soliman Alkhatib[3]

Abstract

The tuned mass-damper-inerter (TMDI) is a newly developed passive energy dissipation unit that combines the conventional tuned mass-damper (TMD) with an inerter mechanism to attenuate undesirable vibrations. This study provides a comprehensive evaluation of the impact of TMDI on the structural response of linear-behaving multi-degree-of-freedom (MDOF) structures subjected to far- and near-fault earthquake-induced ground shaking. The chosen near-fault records guarantee motions with forward directivity (FD) and motions with fling step (FS). An approach based on a genetic algorithm (GA) is used to tackle the optimization problem. The controlled response's objective function is focused on two key factors that are studied separately: minimization of inter-story drifts and minimization of horizontal peak floor acceleration. It is analytically demonstrated that the TMDI performs better than the conventional TMD for relatively small mass ratios, regardless of the distance from a fault rupture. However, the TMD's high-mode dampening effect can be further enhanced by increasing the inertance of the inerter. Additionally, buildings excited by near-fault records with FS have a higher seismic demand on their induced responses. Lastly, the inerter's mass-amplification effect can either enhance the performance of the conventional TMD, for a certain TMD mass, or replace a portion of the TMD's oscillating mass, to realize a substantial weight reduction at a desired level of vibration suppression.

Keywords: Tuned mass damper inerter; Forward directivity; Genetic Algorithm (GA); Optimal design; Near-fault ground motions.
Received: 01 July 2023; Revised: 12 August 2023; Accepted: 16 August 2023.
Article type: Research article

1. Introduction

It is well-known that buildings' safety and functionality can be compromised by unanticipated vibrations caused by winds and earthquake ground motions. These vibrations can cause major damage to the building's elements and ultimately lead to the degradation or collapse of engineering structures. In the conventional practice of seismic design, dynamically excited structures can be easily developed to achieve an acceptable seismic performance limit by applying ductile design and code-prescriptive capacity for earthquake resistance.[1] It is important that the ductility capacities of structural members match the ductility demands imposed on them by the structure's design. Typically, ductility is achieved by enabling the lateral force-resisting system to absorb and dissipate energy in a consistent manner across a significant number of cycles. The components of a structure are designed to have significant, long-lasting deformations in carefully specified locations, preventing the structure from collapsing during a seismic event. As an alternative, passive control systems have been effectively employed to mitigate the effects of wind and earthquake-induced excitations by incorporating energy dissipation devices into structures, thereby reducing the structural responses.[2–4] Passive energy-dissipating systems are simple, inexpensive devices that can be used to safeguard structures from natural hazards and rehabilitate older or defective structures.[5] One distinguishing feature of these effective and widely employed systems is their ability to

[1] *Physics and Engineering Mathematics Department, Faculty of Engineering-Mattaria, Helwan University, Cairo 4034572, Egypt.*
[2] *Faculty of Engineering, King Salman International University, South Sinai, El-Tur, Egypt.*
[3] *Engineering Mathematics and Physics Department, Future University in Egypt, Cairo 11835, Egypt.*
**Email:* aymanm79@hotmail.com (A. Abd-Elhamed)

increase structural energy dissipation by concentrating as much of the dissipated energy as possible into specially designed devices instead of permitting it to accumulate in the main structural members. In order to achieve control over building structures that are excited by dynamic forces, a variety of passive control strategies have been proposed and applied, including passive dampers, seismic isolators, and dynamic vibration absorbers.[6] Passive dampers are manufactured from a diverse range of materials to provide varying levels of stiffness and damping. These dampers are installed within the skeleton of structures such that kinetic energy can be dissipated through the use of viscous fluid, viscoelastic behaviour, and friction in metallic dampers.[7] One of the most significant advances in earthquake engineering in recent decades has been base isolation. It protects both structural elements and non-structural components. Base isolation enables "decoupling" the building from ground movements. By lengthening the structure's fundamental time period and dissipating the earthquake's energy, it lessens the force transmitted to the superstructure. Seismic isolation can be accomplished by using low-stiffness materials located between the structure and its foundation and capable of combining highly elastic behaviour with damping qualities. These materials are used to produce base-isolated structures, which change the structure's fundamental frequency away from its fixed-base frequency and excitation frequency.[8,9] Furthermore, high-dampening rubber bearings act as dampers and add extra damping to the bases of vibration-isolated structures. Dynamic vibration absorbers consist of a top-mounted secondary oscillatory mass whose motion is regulated by optimally designed/tuned stiffeners working in tandem with energy dissipation devices (*i.e.*, viscous dampers).[10] A number of researchers have also studied the seismic performance of TMD-controlled structures[11,12] as well as structures fitted with additional absorber devices like tuned liquid dampers (TLDs)[13–15] and tuned liquid column dampers (TLCDs).[16] Furthermore, studies have been carried out to determine how to boost the dynamic performance of base-isolated structures by employing liquid-based devices such as TLDs[17] and TLCDs.[18] Even though dynamic vibration absorber devices are often used in tall buildings in earthquake-prone areas and have been shown to protect structures from serious dynamic excitation and increase their dynamic responsiveness, they may require a wide space and a lot of weight to be effective. Researchers have demonstrated analytically and numerically that the mass ratio μ, significantly impacts the conventional TMD's ability to suppress vibration.[19] Additionally, a higher μ is associated with significant controlling forces, which leads to larger and more costly TMD support. Nevertheless, for the sake of manufacturing, transportation, installation, and maintenance cost considerations, the μ is typically preselected to be less than 5% of the total building mass. A minimal μ is usually chosen as a solution to the aforementioned problems; however, this severely restricts the TMD's functionality. In recent years, a significant amount of research has been directed toward the development of novel types of TMDs, such as active TMDs, semi-active TMDs, pendulum TMDs, viscoelastic TMDs, multiple TMDs, and "nontraditional" TMDs[20–23] This is done in an effort to make up for the well-known shortcomings of conventional TMDs.

Lieber and Jensen[24] introduced the notion of employing vibrational mass within a container as a means of mitigating vibrations in structures, hence presenting the concept of impact damping technology. The particle damper was subsequently devised by partitioning a single particle into several particles, building upon the principles of the impact damper. Considerable effort has been put into the investigation of potential enhancements to the functionality of traditional particle dampers. Among these is the particle-tuned mass damper (PTMD), which was proposed by Ref. [25] and integrates multiple energy dissipation strategies from both TMDs and particle dampers. The utilization of a finite element method was also suggested as a means to simulate the performance of PTMD. Lu *et al.*[26] introduced a simplified analytical approach to address the limitations associated with the intricate calculations involved in the finite element method. In this proposed method, the authors represented all particles within the PTMD as a single equivalent particle, adhering to specific criteria of equivalence. The authors of the study also introduced a performance-based optimal design approach for PTMDs in the context of nonlinear buildings.[27] Lu and coworkers[28] introduced an improved particle inerter device that exhibits the ability to greatly enhance the vibration control effect of a standard particle tuned mass damper. The findings indicate that the implementation of improved particle inerter device is successful in reducing the displacement and acceleration response of the primary structure.

One of the most popular alternative advancements at the moment can be introduced by combining these dampers with mass-amplification mechanisms like inerter-based devices. This coefficient of proportionality is referred to as inertance (b) and is expressed in mass units. The inerter's technological capabilities allow it to generate a virtual mass hundreds of times greater than the device's actual mass, thereby satisfying the enormous real mass requirement. In this context, the inerter was initially paired with the conventional TMD to construct a device termed the Tuned Mass Damper Inerter,

which was referred to in the relevant body of literature (TMDI). The application of inerter was most common in the field of automotive engineering from the years 2002 to 2010. The floor to which the inerter is grounded is taken into account when calculating the TMDI's performance because this factor has a significant impact on the building's ability to reduce vibration, and in the case where the inerter is grounded to the earth, the absolute acceleration of the corresponding inerter terminal is zero.[29] The installation of the TMDI for base-isolated structures has been investigated, and a more straightforward mathematical formulation for optimizing TMDI designs for these structures has been provided with the objective of decreasing base isolation system displacements during seismic events.[30] Moreover, a number of different criteria that are based on kinematic as well as energy-related indices have been established in order to design the TMDI in the most effective way possible.[30,31] The impact of TMDI placement on performance has been studied by Giaralis and Taflanidis[32] and Ruiz *et al*..[33] The TMDI's installation floor level was not, however, specifically mentioned as a potential optimization target. The effectiveness of TMDIs as a potential solution for minimizing the seismic pounding of nearby low-rise and high-rise buildings has also been investigated by De Domenico *et al*.[34] and Palacios-Quinonero.[35]

Although several studies have claimed that TMDs and TMDIs are effective at controlling the seismic response of structures, the overall validity of these claims is in doubt. One source of uncertainty is the device's reliance on ground motion characteristics for its performance. Such devices are often tuned without consideration of ground tremors. As a result, it is reasonable to assume that their performance in response control may change depending on the type of ground shaking. The literature does not effectively address this ambiguity, and the majority of research only includes results from a small number of ground motions. More specifically, there are limited studies on how to evaluate the performance of control device-equipped buildings in light of the fact that ground motion characteristics can vary. The frequency content of seismic ground motion is one of its key characteristics. It is widely acknowledged that the near field of a rupturing fault can considerably influence the seismic-induced structural response of flexible buildings, such as high-rises and seismically base-isolated structures, etc. (see, for example,[36–38]). These pulse-like ground motions near faults differ dramatically from those seen in the far field. It is known that ground motion recorded near earthquake faults concentrates the majority of its energy in a restricted range of frequencies centred on a dominant or characteristic frequency that closely correlates with the magnitude of the earthquake. Scientists and researchers have identified FD and FS effects as the main characteristics of near-field earthquakes.[39] When seismic waves dispersed by various portions of a rupturing fault arrive at a station, they constructively interfere with one another due to forward-rupture directivity at the source of the seismic.[40,41] This results in the creation of a potent velocity pulse that lasts for only a short period of time. Far-fault ground motions don't have such an obvious pulse. As the rupture propagates toward the seismic recording station, the rupture mechanism, slip direction, and the seismic station's proximity to the fault affect the formation of near-fault ground motion pulses (the "directivity effect").[42,43]). Numerous recent investigations have looked into the consequences that dominant pulses like those described above have on numerous civil engineering structures like buildings, dams, and bridges.[44,45]

Previous studies have shed light on the potentially catastrophic errors that can occur in probabilistic structural fragility analysis as a result of a fundamental omission: the effect of pulse period when considering excitations that are pulse-like. In light of this, Yang *et al*.[46] conducted research to investigate the potential bias of conventional structural seismic fragility for bridge structures when subjected to pulse-like ground motions. Substantial studies on the seismic capacity and response under near-fault ground motions have been conducted by Yang *et al*.[47] and Zhong *et al*.[48,49] and the results demonstrate that the pulse effect of near-fault ground motions has a significant effect on the structure. Additional studies on the efficiency of TMDs in minimizing the impacts of pulse-type ground vibrations on structures are provided in Ref. [50,51]. They discovered that TMD with a low μ is ineffective and may possibly exacerbate the response in some circumstances. According to their observations, low-mass TMD is ineffective and may potentially exacerbate the response.

This research examines the seismic responses of structures equipped with inerter-based vibration suppression devices and compares their performance in the time domain to that of conventional TMD. Consideration is also given to the coupling of TMD with an inerter device, which acts as a mass amplifier to minimize the mass of TMD in seismically excited systems. It was motivated by the above-mentioned issues, which include being susceptible to pulse-like ground motion effects and requiring a large mass in order to be effective in earthquakes. In addition, the impacts of near-fault earthquakes, both those with and without pulses, were not individually assessed for the design of structures in the current version of seismic design codes. Thus, there is a lack of reliable information on their seismic design in the near-fault seismic zone. For this purpose, the TMDI's efficacy is measured by

evaluating the performance of an optimally controlled three-story base-excited structure modelled as an inelastic lumped mass system under far-fault and near-fault earthquakes with FD and FS, picked from three stations' records of the 1999 Chi-Chi earthquake. Closed-form solutions are derived to obtain the response demands for controlled and uncontrolled structures for each ground motion. In addition, techniques that are based on genetic algorithms have been used in the process of tuning TMDs and TMDIs that are located on the upper stories of high-rise structures. Taking into account predefined values for μ and inertance ratio (β), the optimal values for the design parameters such as the frequency ratio ($\boldsymbol{\upsilon}$) and the damper critical damping ratio ($\boldsymbol{\xi}$) that result in the smallest displacement response as objective functions are derived.

2. Ground motion records

The near-fault ground motion records from the 1999 Chi-Chi earthquake have been chosen for this study's input ground motion. In addition, another earthquake record is picked to highlight characteristics of far-fault ground motion detected at the same site condition during the same earthquake occurrence with a distant epicentre recorded under identical site conditions. The near-fault ground motion records are categorized into the directivity pulse and the pulse associated with permanent displacement based on the rupture process and the accompanying rupture directivity effect. A dynamic phenomenon known as forward directivity occurs when the rupture front travels toward the site and the fault slips parallel to it. This happens where the fault rupture moves at a velocity that is similar to the velocity of the shear wave. For strike-slip faults, the displacement related to such a shear-wave velocity is the greatest in the fault-normal direction[42] and is typically detected in the velocity or displacement time history.[43] On the other hand, the ground motions near the surface fault rupture may include perpetual ground displacement, which is known as FS and produces pulses of unidirectional velocity. This possibility is contingent on the site's ground displacement.

The time histories of the responses caused by the Chi-Chi earthquake are shown in Fig. 1. These time histories are depicted in terms of displacement, velocity, and acceleration. In addition to that, the spectra of the response as well as the Fourier amplitude for both far- and near-fault ground motions are also presented. The following three sites were chosen to capture earthquake motion recordings for the Chi-Chi earthquake: HWA032, TCU068 and TCU065. These three stations stand for ground motions associated with far-fault, near-fault with FS, and near-fault with FD, respectively. In Table 1, there are detailed descriptions of the various ground motions as well as their respective characteristics. It is abundantly evident from looking at Fig. 1 that there is a notable disparity between the records that were chosen. In addition, the figure illustrates the difference between the ground motion records in terms of the existence of velocity pulses. However, the earthquake that occurred near the fault and had FS had a long-period velocity pulse that was just on one side. In addition, a step that resembles a ramp can be seen in each of the presented displacement time histories. This step is what distinguishes the FS records' displacement time histor Further study is required y. The ground motion records for the near-fault earthquakes as well as the far-fault earthquakes have both been adjusted to make the PGA equal to 0.3 g.

Table 1. Near-fault and far-fault ground motion characteristics for 1999 Chi-Chi earthquake.

Ground motion	Recorded station	Mw	Dss (km)	PGA (g)	PGV (m/s)
Far-fault	HWA032,	7.62	47.31	0.15	0.082
Near-fault with FS	TCU068	7.6	3.10	0.37	2.78
Near-fault with FD	TCU065	7.6	0.6	0.79	1.26

Mw = Magnitude; Dss = site-source distance; PGA = Peak Ground Acceleration; PGV = Peak Ground velocity.

3. Mathematical model for TMDI equipped multi-storey structures

A diagrammatic illustration of the structural system with lumped masses excited by a horizontal ground acceleration $\ddot{x}_g$, both with and without TMDI units, is depicted in Fig. 2. The TMDI is a passive vibration-suppression device that is modelled as an additional SDOF. It comprises a conventional TMD that is positioned on the top floor level to mitigate seismic-induced responses. The secondary mass m_{TMDI} is connected to the structure by a spring with a stiffness of k_{TMDI} and a dashpot with a damping value of c_{TMDI}. As shown in Fig. 2, a green-highlighted inerter device with inertance b connects the TMD oscillating mass to the floor beneath the roof.

It is assumed that the TMDI's pendulum mass is suspended from the structure's roof. The pendulum mass is attached to one terminal of the inerter, and the ground or any other arbitrary structural mass is connected to the other terminal.[52] It has been discovered that the inerter functions most effectively when it is connected to the earth. This is due to the fact that, in this configuration, the inerter force is proportional to the absolute acceleration of only the pendulum mass, but it is not proportional to the relative acceleration of the two inerter terminals.[53]

The inerter device is modelled by a negligible mass element linking two free-moving nodes; as a result, it produces a force

proportional to its terminals' relative acceleration. In this regard, the resisting inerter force can be expressed as follows:

$$F_{iner}(t) = b[\ddot{x}_{TMDI} - \ddot{x}_f] \quad (1)$$

where x_{TMDI} represents the auxiliary oscillating mass's lateral displacement, x_f represents the floor's lateral displacement to which the inerter links the auxiliary mass, and a dot over a symbol denotes differentiation with respect to time. Consequently, in the TMDI configuration, the inerter contributes to the primary structure's mass-related inertial force, Fb, whose amplitude is influenced by the inerter terminals' relative acceleration and inertance b.

The controlled MDOF shear building is subjected to a seismic horizontal base acceleration, and the governing equation of motion is expressed as a matrix as follows:

$$M\ddot{X}(t) + C\dot{X}(t) + KX(t) = -MI\ddot{x}_g(t) \quad (2)$$

where $\boldsymbol{M}$, $\boldsymbol{C}$ and $\boldsymbol{K}$ respectively represent the standard dynamic characteristic matrices for mass, damping, and stiffness of the building model, modified by the inclusion of the TMDI, as illustrated Eqs. (3) – (5). The vectors $\boldsymbol{X(t)}$, $\boldsymbol{\dot{X}(t)}$ and $\boldsymbol{\ddot{X}(t)}$; respectively denote the fundamental structure's generalized displacement, velocity, and acceleration, respectively. $\boldsymbol{\ddot{x}_g(t)}$ is a vector denoting the ground acceleration. Finally, $\boldsymbol{I}$ is the influence vector.

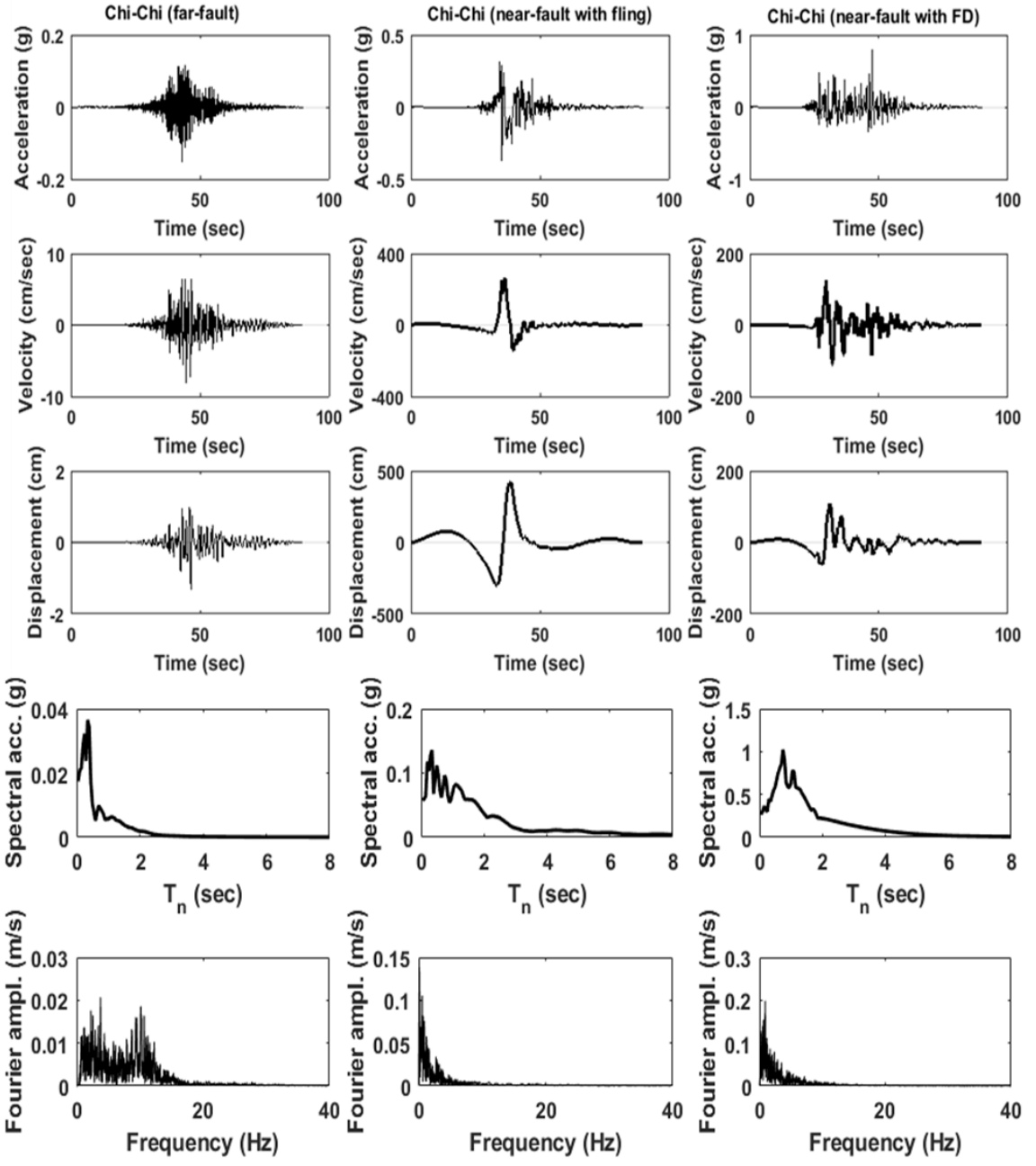

Fig. 1 The time-histories acceleration, velocity, displacement, response spectra and Fourier amplitude for (a) far-fault ground motion captured at HWA032 station, (b) near-fault with FS ground motion captured at TCU068 station and (c) near-fault with FD ground motion captured at TCU065 station in 1999 Chi-Chi earthquake.[12]

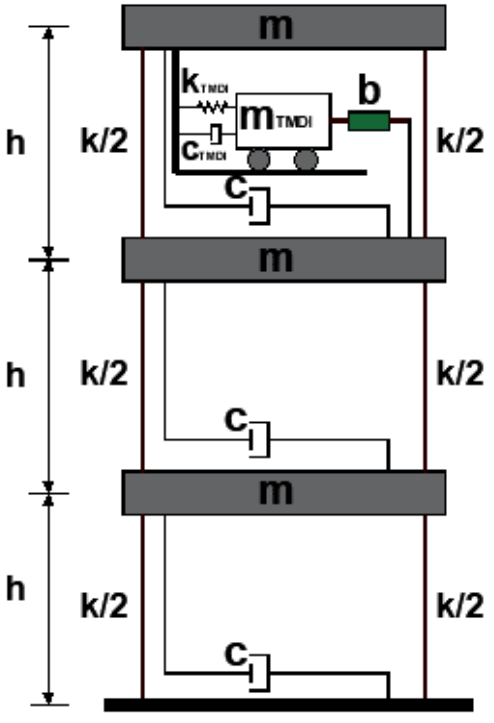

Fig. 2 A schematic diagram of the TMDI-equipped multi-storey structure. The blue and green blocks indicate the mass and inerter, respectively.

$$M = \begin{bmatrix} m_1 & 0 & 0 & 0 \\ 0 & m_2 + b & 0 & -b \\ 0 & 0 & m_3 & 0 \\ 0 & -b & 0 & m_{TMDI} + b \end{bmatrix} \quad (3)$$

$$C = \begin{bmatrix} c_1 + c_2 & -c_2 & 0 & 0 \\ -c_2 & c_2 + c_3 & -c_3 & 0 \\ 0 & -c_3 & c_3 + c_{TMDI} & -c_{TMDI} \\ 0 & 0 & -c_{TMDI} & c_{TMDI} \end{bmatrix} \quad (4)$$

$$K = \begin{bmatrix} k_1 + k_2 & -k_2 & 0 & 0 \\ -k_2 & k_2 + k_3 & -k_3 & 0 \\ 0 & -k_3 & k_3 + k_{TMDI} & -k_{TMDI} \\ 0 & 0 & -k_{TMDI} & k_{TMDI} \end{bmatrix} \quad (5)$$

In addition, the expressions below comprise the components of the response vectors:

$$X = \begin{bmatrix} x_1 \\ x_2 \\ x_3 \\ x_{TMDI} \end{bmatrix}, \dot{X} = \begin{bmatrix} \dot{x}_1 \\ \dot{x}_2 \\ \dot{x}_3 \\ \dot{x}_{TMDI} \end{bmatrix}, \ddot{X} = \begin{bmatrix} \ddot{x}_1 \\ \ddot{x}_2 \\ \ddot{x}_3 \\ \ddot{x}_{TMDI} \end{bmatrix} \quad (6)$$

It is worth noting that when $b = 0$, Eqs. (2–6) govern the response of conventional TMD-equipped MDOF building structures attached to the upper floor level. Furthermore, because the inertance b only alters the mass matrix, which is no longer diagonal, the inerter could be immediately incorporated into the building's equations of motion. In addition to this, Eq. (3) demonstrates that the total inertia of the TMDI is equivalent to $(m_{TMDI} + b)$.

The three non-dimensional design parameters chosen to best characterize the TMDI are the μ, $\boldsymbol{\upsilon}$, and $\boldsymbol{\xi}$, which can be defined as follows:

$$\mu = \frac{m_{TMDI}}{M_s}, \ \upsilon = \frac{\omega_{TMDI}}{\omega} = \frac{\sqrt{\frac{k_{TMDI}}{m_{TMDI}+b}}}{\sqrt{\omega}}, \ \xi = \frac{c_{TMDI}}{2(m_{TMDI}+b)\omega_{TMDI}} \quad (7)$$

where M_s and ω represent the primary structure's total mass and first natural frequency, respectively,

Also, a new dimensionless parameter, namely inertance ratio β, represented by the ratio of the inerter constant b over the fundamental structure's mass, is introduced hereunder.

$$\beta = \frac{b}{M_s} \quad (8)$$

Typically, the frequency and damping ratios are regarded to be optimization variables, whereas the mass and inertance ratios are specified as constants in advance.

4. Exact analytical formulation

To obtain the closed-form solution for the seismic response of uncontrolled buildings subjected to far- and near-fault earthquake records, the ground acceleration illustrated in Fig. 1 is modelled using unit step functions $U(t-\tau)$ along subintervals of extremely short length τ.[54] Therefore, the following series form of unit-step functions can be used to express the interpolating function $\ddot{u}_g(t)$.

$$\ddot{x}_g(t) = \sum_{i=1}^{\infty}[\, U_i(t) - U_{i+1}(t)\,]\ddot{u}_g(\tau_i) \quad (9)$$

where the unit step function is $U_i(t) = U(t-\tau_i) = \begin{cases} 1; & t \geq \tau_i \\ 0; & t < \tau_i \end{cases}$ and $\tau_i = i\tau$.

Incorporating Equation (9) into Equation (2) yields

$$M\ddot{X}(t) + C\dot{X}(t) + KX(t) = -M_1 \sum_{i=1}^{\infty}[\, U_i(t) - U_{i+1}(t)\,]\ddot{u}_g(\tau_i) \quad (10)$$

Typically, a structure's dynamic analysis starts with a static condition. This means that the initial displacement and velocity are both at zero at the starting time, as will be shown in the following.

$$X_1(0) = \dot{X}_1(0) = X_2(0) = \dot{X}_2(0) = \cdots = X_n(0) = \dot{X}_n(0) = 0. \quad (11)$$

Substituting $\ddot{u}_g(t)$ from Eq. (11) into Eq. (2) and applying the Laplace transform to the resulting equation with the aid of Eq. (11) yields,

$$(m_1 s^2 + (c_1 + c_2)s + (k_1 + k_2))U_1(s) + (-c_2 s - k_2)U_2(s) = -m_1 U_g(s) \quad (12)$$

$$(-c_2 s - k_2)U_1(s) + (m_2 s^2 + (c_2 + c_3)s + (k_2 + k_3))U_2(s) + (-c_3 s - k_3)U_3(s) = -m_2 U_g(s) \quad (13)$$

$$(-c_3 s - k_3)U_2(s) + (m_3 s^2 + c_3 s + k_3)U_3(s) = -m_2 U_g(s) \quad (14)$$

where

$$U_g(s) = \sum_{i=1}^{\infty} \ddot{U}_g(\tau_i)(e^{\tau_i s} - e^{-\tau_{i+1} s}) \quad (15)$$

The linear system Eqs. (12-14) can be written as

$$\mathrm{AU} = \mathrm{B} \quad (16)$$

where

$$\boldsymbol{A}=\begin{bmatrix} sc_1+sc_2+k_1+k_2+s^2m_1 & -sc_2+k_2 & 0 \\ -sc_2+k_2 & sc_2+sc_3+k_2+k_3+s^2m_2 & -sc_3-k_3 \\ 0 & -sc_3-k_3 & sc_3+k_3+s^2m_3 \end{bmatrix},$$

$$\boldsymbol{b}=\begin{bmatrix} m_1 \\ m_2 \\ m_3 \end{bmatrix} U_g(s). \tag{17}$$

also, the unknowns are the functions $U_j(s)$, $j=1,2,\cdots,n$, given by

$$U_j(s)=\left[\left(s^{2n-2}+\sum_{k=1}^{2n-2}\beta_{jk}s^{2n-2-k}\right)/(s^{2n}+\sum_{k=1}^{2n}\alpha_k s^{2n-k})\right]U_g(s), \tag{18}$$

which is rewritten as follows

$$U_j(s)=\left[\sum_{k=1}^{n}\frac{A_{jk}^*s+B_{jk}^*}{s^2+k_k^*s+h_k^*}\right]U_g(s), \tag{19}$$

Applying the inverse Laplace transform to Equation (19), the closed-form solution is obtained, which is as follows:

$$u_j(t)=\sum_{i=1}^{\infty}\ddot{u}_g(\tau_i)\left[\sum_{k=1}^{2}\left[e^{-k_k^*t/2}\left[e^{k_k^*\tau_{i+1}/2}\left[f_{jk}(t-\tau_{i+1})+g_{jk}(t-\tau_{i+1})\right]U_{i+1}(t)-e^{k_k^*\tau_i/2}\left[f_{jk}(t-\tau_i)+g_{jk}(t-\tau_i)\right]U_i(t)\right]\right]\right], \tag{20}$$

where

$$f_{jk}(T)=A_{jk}^*\cosh(b_kT),\ g_{jk}(T)=\frac{a_{jk}}{2b_k}\sinh(b_kT),\quad a_{jk}=2B_{jk}^*-k_k^*A_{jk}^*,\ b_k=\frac{1}{2}\sqrt{(k_k^*)^2-4h_k^*}, \tag{21}$$

T is a dummy variable, $j=1,2,3$ and $k=1,2,3$.

5. Optimal TMDI parameters

After the dynamic vibration equations of seismically excited structures have been established, it will be feasible to find the optimal values for the TMDI design parameters. This will allow the structures to vibrate with the least amount of disturbance possible. The tuning procedure was carried out by utilizing an approach based on a genetic algorithm in conjunction with a time history analysis. During this process, two strategic parameters were minimized individually as objective functions. These parameters included the minimization of inter-story drifts and horizontal peak floor acceleration. Therefore, the following characteristics describe these two methods of optimization: $J_{obj1}=\min(\max(|Max.storey\ drift|))$ and $J_{obj2}=\min(\max(|Storey\ acc.|))$.

Consequently, the TMDI devices' frequency tuning and damping ratio were fine-tuned for this purpose. The optimal design problem under consideration calls for the simultaneous optimization of four independent design parameters, each of which is dimensionless: the vector $g_1=[\upsilon\quad \xi]^T$ contains the TMDI frequency as well as the damping ratios grouped together, and the ratios of mass and inertance, which are gathered into the vector $g_2=[\mu\quad \beta]^T$.

The genetic algorithm (GA) is utilized in order to accomplish the optimization of the control device settings. The utilization of this approach is applicable in addressing many optimization issues that are not ideally suited for conventional optimization techniques. These problems may involve objective functions that exhibit stochastic behavior, lack differentiability, possess discontinuities, or exhibit significant levels of nonlinearity. In recent times, there has been a surge in the use of genetic algorithms for addressing civil engineering challenges, mostly owing to their inherent capacity, adaptability, and efficiency. MATLAB's Genetic Algorithm (GA) is utilized to solve the optimization problem numerically in order to identify the optimal design parameters in g_1 that are constrained to the predetermined search range $[g_1^{min}, g_1^{max}]$ for various provided values of the parameters in g_2. This can be written in mathematical form as:

$$\underbrace{min}_{g_1}[\mathrm{OF}(g_1 \mid g_2)],\ \text{where OF}=peak\{responses\},$$
$$\text{subjected to } g_1^{min}\le g_1\le g_1^{max} \tag{22}$$

With the secondary design parameters MR and β, the aforementioned optimal design formulation makes it possible to take into account any required combination of the TMDI's inertial properties, that is, attached mass and inertance. Additionally, the subsequent numerical work is focused on determining the optimal υ and $\boldsymbol{\xi}$ values for a given set of μ and β values. This is referred to as the tuning phase. Consequently, to rule out the chance that the optimal design values are beyond the search domain, the boundaries of the search scope utilized in solving Eq. (22) are chosen as $g_1^{min}=[0.5\ 0.01]^{\mathrm{T}}$ and $g_1^{max}=[2\ 0.5]^{\mathrm{T}}$.

The following is a consideration of the range of preselected values while using Matlab's vector notation:

μ = [0.02: 0.03: 0.05: 0.1], *and* β = [0: 0.25: 0.5: 0.75].

A flowchart describing the approach suggested in this study for the determination of the optimal TMDI device design parameters is depicted in Fig. 3. These parameters influence the response of a structure when it is subjected to seismic excitation.

The TMDI parameters selection procedure can get off to a good start by using these ranges, which are common for conventional TMDs and constitute a reasonable starting point. The optimum tuning values established by the suggested method for various system parameter values are listed in Table 2 and Table 2 for design parameters derived from J_{obj1} and J_{obj2}, respectively with regard to the building model that was previously provided.

It should be pointed out that the quantitative results that are presented in Table 2 for the conventional TMD are in agreement with other results that have been reported in the literature that were obtained by employing different numerical optimization strategies. To be more specific, larger TMD masses necessitate larger $\boldsymbol{\xi}$ values and smaller TMD $\boldsymbol{\upsilon}$s for optimal tuning.

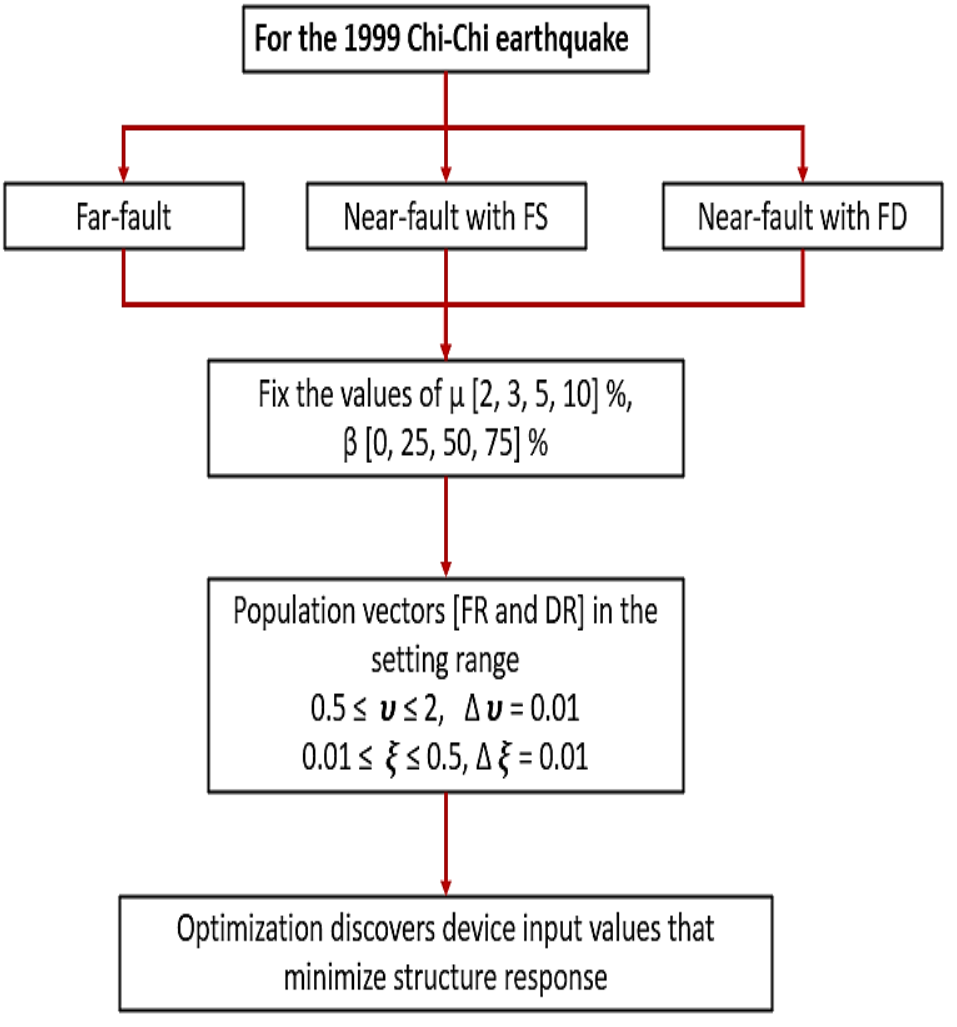

Fig. 3 Flowchart of the proposed optimization approach.

Table 2. Optimization results for J_{obj1} using the proposed approach for varying TMD mass and inertia ratio for system subjected to Chi-Chi earthquake.

m_{TMDI} (kg)	β (%)	Far-fault		Near-fault with FS		Near -fault with FD	
		υ	ξ	υ	ξ	υ	ξ
	0	0.9341	0.0953	0.9538	0.0723	1.172	0.0938
1500	25	0.8192	0.0871	0.8983	0.0681	1.293	0.1354
[μ = 2%]	50	1.1521	0.0998	1.0619	0.0658	1.412	0.1471
	75	1.2194	0.1535	1.143	0.0878	1.543	0.1544
	0	0.8823	0.0165	0.7965	0.0175	0.9716	0.9365
2250	25	0.9965	0.0176	0.8666	0.0198	1.105	0.1172
[μ =3%]	50	1.1261	0.0201	0.9268	0.0213	1.111	0.1275
	75	0.8745	0.0223	0.9884	0.0265	1.256	0.1635
	0	0.8186	1.016	0.8523	0.0193	1.102	0.0954
3750	25	0.9952	1.212	0.8743	0.0185	1.287	0.1827
[μ = 5%]	50	1.145	1.302	0.9657	0.0277	1.393	0.1294
	75	1.367	1.586	1.0394	0.0294	1.414	0.1364
	0	0.9851	0.1783	0.8631	0.1231	0.9716	0.2342
7500	25	1.116	0.1933	0.9274	0.1363	1.105	0.3303
[μ = 10%]	50	1.238	0.2342	1.4267	0.1989	1.1114	0.3334
	75	1.365	0.2876	1.3442	0.2745	1.2846	0.4867

Table 3. Optimization results for J_{obj2} using the proposed approach for varying TMD mass and inertia ratio for system subjected to Chi-Chi earthquake.

		Far-fault		Near-fault with FS		Near -fault with FD	
m_{TMDI} (kg)	β (%)	$\boldsymbol{\upsilon}$	$\boldsymbol{\xi}$	$\boldsymbol{\upsilon}$	$\boldsymbol{\xi}$	$\boldsymbol{\upsilon}$	$\boldsymbol{\xi}$
	0	0.5342	0.0231	0.7354	0.0091	1.0379	0.0991
1500	25	0.9154	0.0041	1.0586	0.0387	0.9287	0.1047
[μ = 2%]	50	0.7381	0.1798	0.7325	0.1709	1.0554	0.1161
	75	1.0723	0.1506	0.0889	0.1888	0.9668	0.1452
	0	0.9668	0.0639	0.8777	0.0666	1.0539	0.1728
2250	25	0.7485	0.0840	0.9960	0.0840	1.3761	0.1618
[μ =3%]	50	1.0539	0.1452	1.0586	0.0991	1.3768	0.1798
	75	0.6252	0.1522	1.1548	0.1161	1.4687	0.1594
	0	0.8358	0.1231	0.8921	0.0231	1.5730	0.0035
3750	25	1.1027	0.1658	1.1135	0.0813	1.9680	0.3563
[μ = 5%]	50	1.2507	0.2355	1.2074	0.1224	1.9926	0.3853
	75	1.9932	0.2485	1.9945	0.1423	1.9680	0.4141
	0	1.9680	0.0187	1.0254	0.0785	0.9154	0.3049
7500	25	1.1326	0.4817	1.3915	0.2566	1.2074	0.423 2
[μ = 10%]	50	1.9954	0.48394	1.9432	0.0007	0.9657	0.47598
	75	1.9986	0.4858	0.6281	0.2766	1.2074	0.4766

6. Numerical studies

To illustrate the external passive vibration control device's viability and efficacy in reducing the vibration of existing structures, the control performance of a three-story building model equipped with TMD (β=0) and TMDI is extensively investigated in this study using Chi-Chi ground motion records, namely, far-fault, near-fault with FS, and near-fault with FD. For the seismic analysis, the three-story building of equal height is properly considered. The building model's lumped mass and lateral stiffness for each story are 25×10^3 kg and 3.46×10^6 N/m, respectively. The fundamental period is 1.2 s. (see[55,56]) The results of a conventional modal analysis reveal that the undamped natural frequencies of the considered main building are as follows: ω_1 = 5.23 rad/s, ω_2 = 14.67 rad/s, and ω_3 = 21.19 rad/s. For the first, second, and third stories, the fundamental modes of vibration are 0.4450, 0.8019, and 1.00, respectively, when normalized to the displacement of upper floor displacement. Additionally, it is assumed that the damping ratio ξ for the building as a whole is equal to 0.02, which results in the building stories' damping coefficient being C = 6.609 Ns/m.[57] The TMDI device's $\boldsymbol{\upsilon}$ and $\boldsymbol{\xi}$ were tuned in the analysis to reduce the roof displacement of the MDOF structure under consideration when subjected to near and far-fault ground motions. A single-objective minimization technique was used to optimize the TMDI's parameters. The displacement at the top of the structure was the objective function that needed to be minimized. The optimization issue was resolved using a MATLAB-implemented Genetic Algorithm (GA). In order to explore the findings, we first examine the performance of conventional TMD and then the performance of TMDI under various types of ground motions to ascertain how the peculiarities of the ground motions affect the performance of TMD and TMDI.

6.1 Performance of a TMD-equipped structure

A free-to-vibrate mass is typically employed as a passive vibration control unit to reduce the oscillatory motion generated by seismic excitations. Under far-fault and near-fault earthquake excitations, the effectiveness of TMD in suppressing earthquake-induced vibrations is examined in the time domain. Let the TMD mass be 3750 kg, which is 5% of the 3-DOF basic structure's overall mass. Therefore, for far-fault records, the optimal design TMD parameters for $\boldsymbol{\upsilon}$ and $\boldsymbol{\xi}$ used in the analysis are 0.7965 and 0.07531, and for near-fault with FS records, they are 0.8153 and 0.0974. For near-fault with FD records, the $\boldsymbol{\upsilon}$ and $\boldsymbol{\xi}$ are 1.016 and 0.0869, respectively.

Figure 4 shows the first, second, and third story horizontal displacement time-histories of the MDOF building model in Fig. 2 with and without TMD under the Chi-Chi earthquake records as far-fault, near-fault with FS, and near-fault with FD. As anticipated, the maximum displacement responses from the top floors are much higher than those from the lower floors. The presented plots unmistakably show that for all the taken earthquake recordings, the controlled building exhibits noticeably lower displacement responses than the uncontrolled one. According to Fig. 4, increasing the height of the story increases the disparity between the plots obtained for the controlled and uncontrolled building models for all seismic records taken into account throughout the analysis. Nevertheless, the greatest displacement responses are brought about for all building stories by the near-fault with FS ground motion. It's also noteworthy to observe that the uncontrolled structure's peak response occurs significantly later than the peak ground velocity where the control system is appropriate against ground motions containing numerous strong cycles of velocity pulses. According to the predicted peak displacement

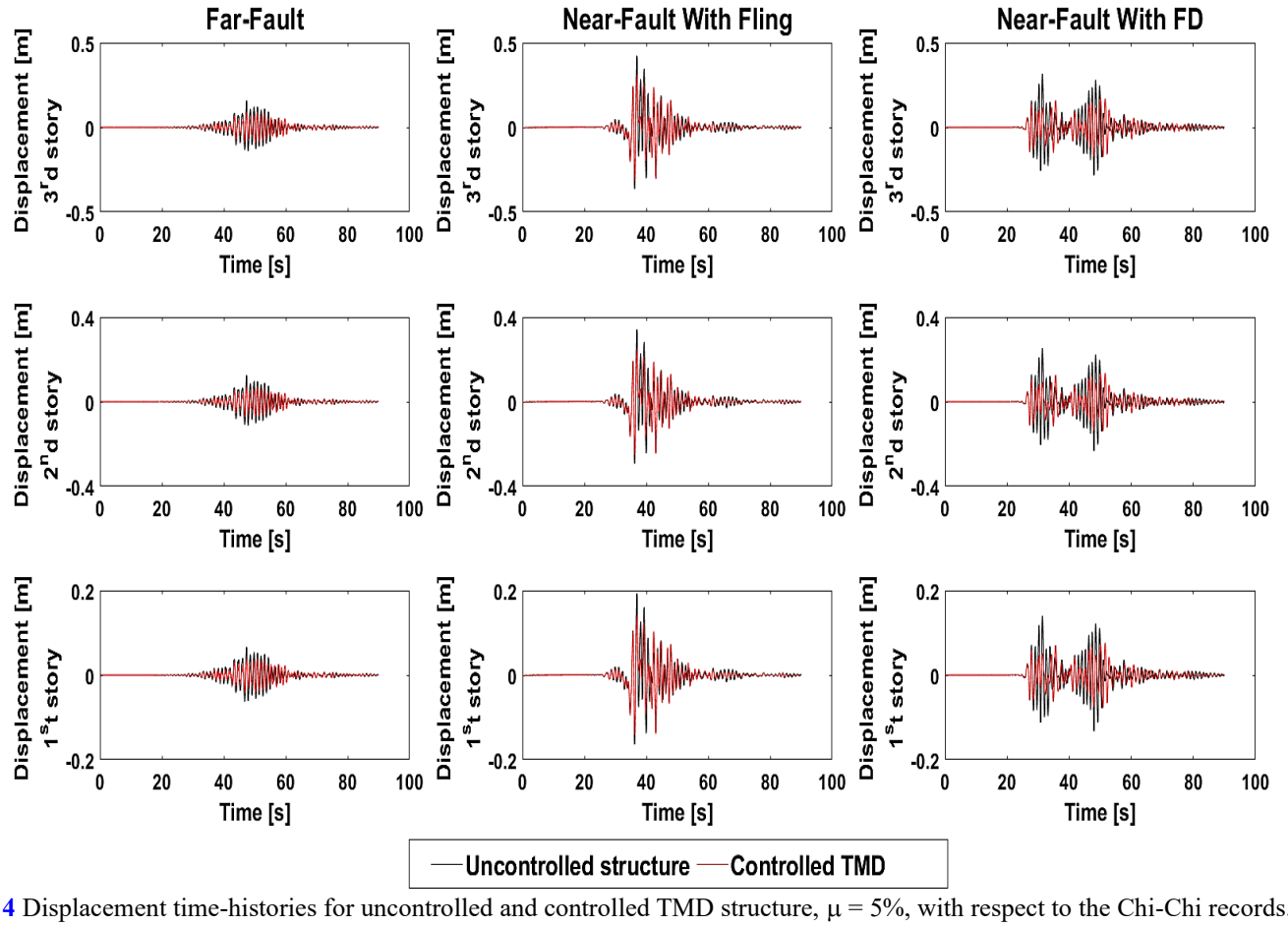

Fig. 4 Displacement time-histories for uncontrolled and controlled TMD structure, μ = 5%, with respect to the Chi-Chi records.

responses, the first, second, and third storeys of the uncontrolled building model that was subjected to the Chi-Chi earthquake's far-fault records saw peak storey displacement values of 0.0666, 0.1247, and 0.1586 m, respectively. The TMD-equipped building's equivalent peak values are 0.0418, 0.0738, and 0.093 m, respectively. The obtained peak storeys displacement values for the same structure under the near-fault with FS and near-fault with FD records of the Chi-Chi earthquake are recorded as 0.1935, 0.3423, 0.4235 m and 0.1400, 0.2529, 0.3163 m for the 1st, 2nd, and 3rd storeys, respectively. The controlled building model's corresponding peak values are 0.1434, 0.2531, 0.1391 m, and 0.0782, 0.1391, 0.1759 respectively. The results demonstrate that integrating the TMD significantly reduces the induced displacements for both near and far-fault ground motions. Thus, if the optimal parameters are carefully chosen, TMD can be a more effective and potentially useful device for controlling the structure's response.

6.2 Performance of a TMDI-equipped structure

This section provides additional numerical results to illustrate the TMDI's mass amplification effect and to evaluate the TMDI's effectiveness as a structural passive vibration control strategy for multi-structure systems in comparison to the conventional TMD. To actually achieve this, the peak values of the displacement time histories of the storeys for the previously considered 3-story building model equipped with a TMD with μ = 5% of the structure's total mass and an inertance ratio β = 0 and a TMDI with the same attached mass and assuming an inertance ratio β =25% under far- and near-field records with FS and FD as seismic excitations are determined. Fig. 5 exhibits the peak values of storeys displacements for the uncontrolled and TMD-controlled MDOF building models. These values are compared to those of the TMDI-controlled building model, which was obtained from the same far- and near-field earthquake records. From Fig. 5, it is clear that the peak displacements increase as the building's height increases, with the highest displacements corresponding to near-fault ground motion. However, according to the simulation's findings, the near-fault with FS records had larger induced peak displacement values than the near-fault with FD and the far-fault records. This could be a result of the two near-fault earthquake motions, both of which contain significant, rapid ground displacements as a result of near-source effects (see Fig. 1). Observations indicate that the disparity between uncontrolled and controlled structures' lateral peak storey responses during near-fault ground motion widens more as the story height increases than the disparity obtained during far-fault ground motion.

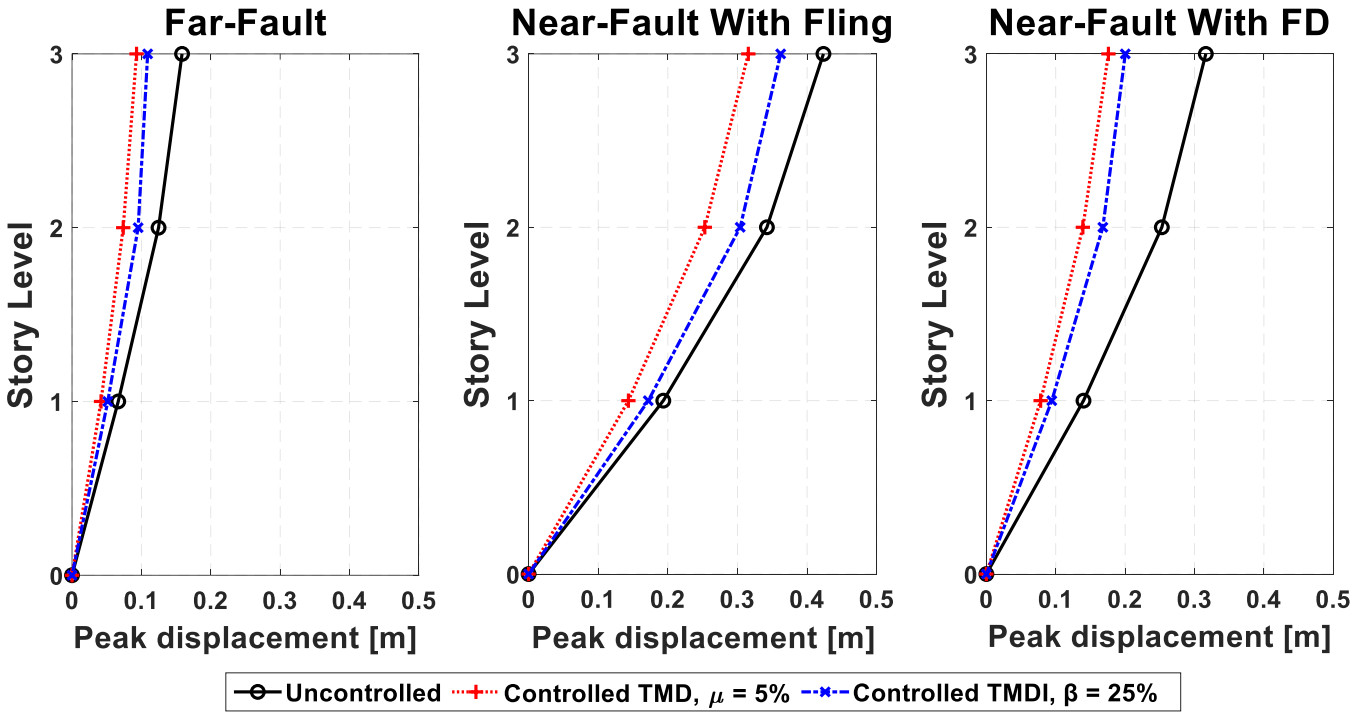

Fig. 5 Peak displacement at each story level for uncontrolled, controlled TMD, μ = 5%, and controlled TMDI, β = 25%, with respect to the Chi-Chi records, design parameters derived from J_{obj1}.

As can be shown from far-fault records of the Chi-Chi earthquake, the lead mass of the uncontrolled building model m_3 experiences a peak displacement of 0.1586 m. With the TMD, the peak displacement is reduced to 0.093 m, and with the TMDI, it is reduced to 0.109 m, which is a reduction of 41% and 31%, respectively. The uncontrolled building model's lead mass m_3's peak displacement is 0.4235 m under the Chi-Chi earthquake's near-fault with FS. The TMD reduces the peak displacement to 0.3156 m and the TMDI to 0.3621 m, representing reductions of 25% and 18%, respectively. However, uncontrolled peak storey displacement of the building model's lead mass m_3 under Chi-Chi near-fault FD is 0.3163 m. The TMD reduces peak displacement by 44% and the TMDI by 21%. These results show that the TMD device is more effective than the TMDI device at reducing the peak displacement responses of the MDOF building model. Furthermore, a significant factor that impacts a building's performance is the dominant pulse frequency. The TMDI control device's undesirable behavior is related to the seismology characteristic of ground motions.

One of the most important indicators of structural behaviour in performance-based seismic studies is "story drift," which is the lateral displacement of a single level relative to the level above or below normalized by floor height. Story drift over certain thresholds might cause structural damages. Under the far-fault and near-fault records of the Chi-Chi earthquake, Fig. 6 depicts the curves of stories drift for the uncontrolled and controlled MDOF building models considering the results obtained from J_{obj1} and J_{obj2}. As depicted in the figure, for the three applicable earthquakes, the drift distribution achieved its greatest value at around one-third the height of the investigated building models. Compared to the other two controlled models, the uncontrolled model displays a noticeable change in the induced storey drift. As seen in the figure, near-fault earthquake motion with FS induces higher peak storey drifts than far- and near-fault earthquake motion with FD records. In addition, the storey drifts that were derived from the far-fault records are quite close to one another and do not deviate substantially from one another. However, the storey drifts at the lower stories as a result of the far- and near-fault records are higher than those at the upper storeys. In Fig. 6(a) the maximum drift response obtained for the uncontrolled building model subjected to the far-fault, near-fault with FS, and near-fault with FD is 0.0234, 0.0658, and 0.0477, respectively, and the corresponding values for the building equipped with a TMDI are 0.0175, 0.0594, and 0.0327. The maximum drift is reduced to 0.0137, 0.0487, and 0.0272 with the TMD-equipped building. In general, the Chi-Chi near-fault ground motion causes a significant difference in the storey drifts, particularly at the lower stories. In Fig. 6(b), using the tuning parameters computed from J_{obj2}, it can be observed that In Fig. 6(a) the maximum drift response obtained for the uncontrolled building model subjected to the far-fault, near-fault with FS, and near-fault with FD is 0.0213, 0.0615, and 0.0462, respectively, and the corresponding values for the building equipped with a TMDI are 0.0174, 0.0613, and 0.0314. The maximum drift is reduced to 0.0136, 0.0472, and 0.0255 with the TMD-equipped building. In general, the Chi-Chi near-fault ground motion causes a significant difference in the storey drifts, particularly at the lower stories.

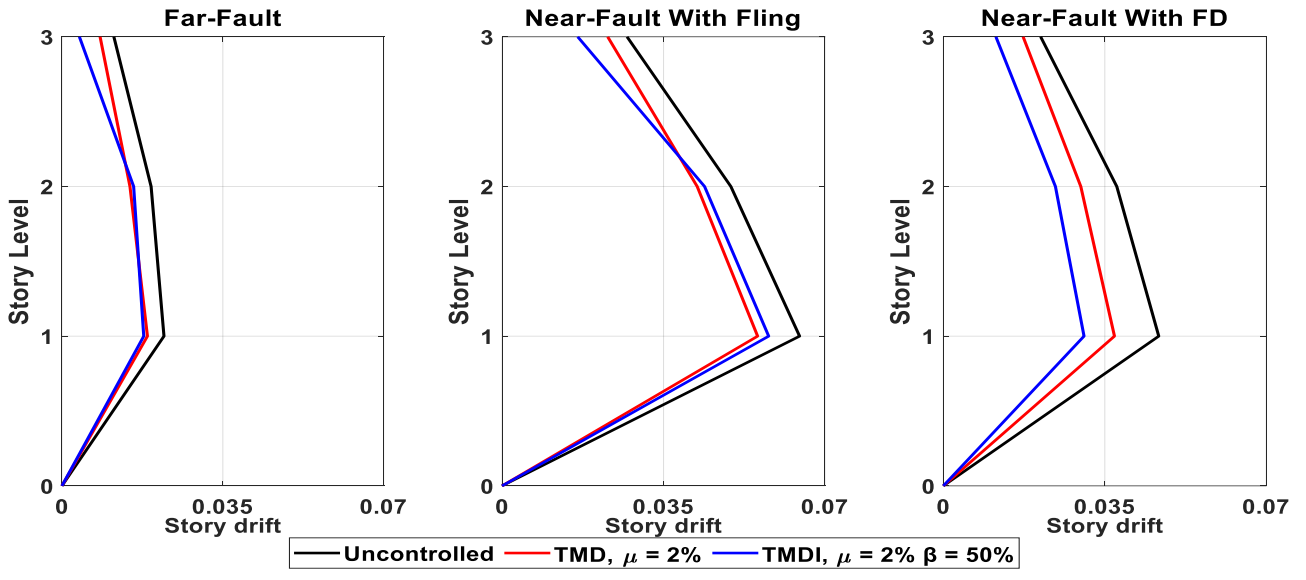

(a) Optimal design parameters derived from *Jobj1* approach.

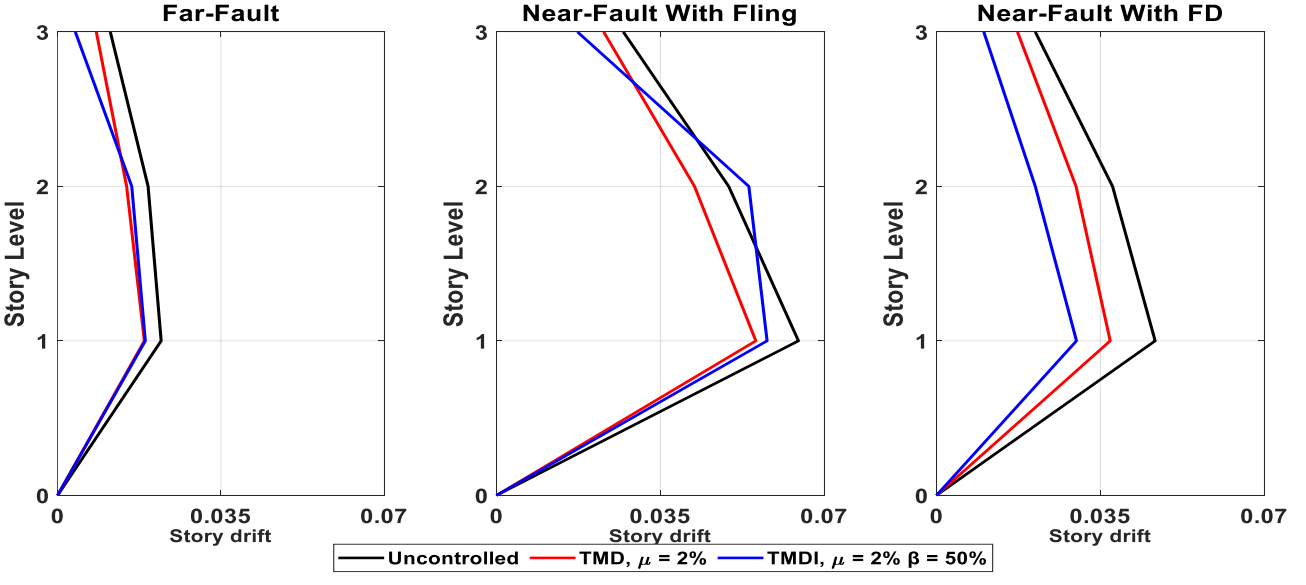

(b) Optimal design parameters derived from *Jobj2* approach.

Fig. 6 Storey drifts along the height for uncontrolled, controlled TMD, μ = 5%, and controlled TMDI, β = 25%, with respect to far- and near-fault records with FS and FD.

Recent years have seen a significant increase in the amount of focus placed on the estimation of floor acceleration for the purpose of assessing seismic demands. It is a significant indicator of damage to non-structural elements as well as the overall performance of the structure. On the other hand, the floor accelerations that develop in the superstructure as a result of seismic ground motion are proportionate to the forces that are exerted as a result of ground shaking. Further, buildings with acceleration-sensitive equipment may find that avoiding excessive floor accelerations is crucial. The acceleration time histories of seismically excited TMD and TMDI-controlled three-story buildings are depicted in Fig. 7 using the tuning parameters computed from J_{obj1}. These buildings were subjected to the Chi-Chi, Far-Fault, Near-Fault with FD, and Near-Fault with fling records, respectively. In addition, a summary of the values of the peak accelerations at each storey level may be found in Table 4. It can be seen from Fig. 7 and Table 4 that the peak-induced acceleration tends to increase with building height. It has been found that the inerter–based TMD influences the peak acceleration responses for all storey levels. As can be seen from the figure, incorporating inerter devices into seismic-excited TMD-equipped buildings leads to a decrease in the peak accelerations of the storeys of the building model for all the considered seismic records.

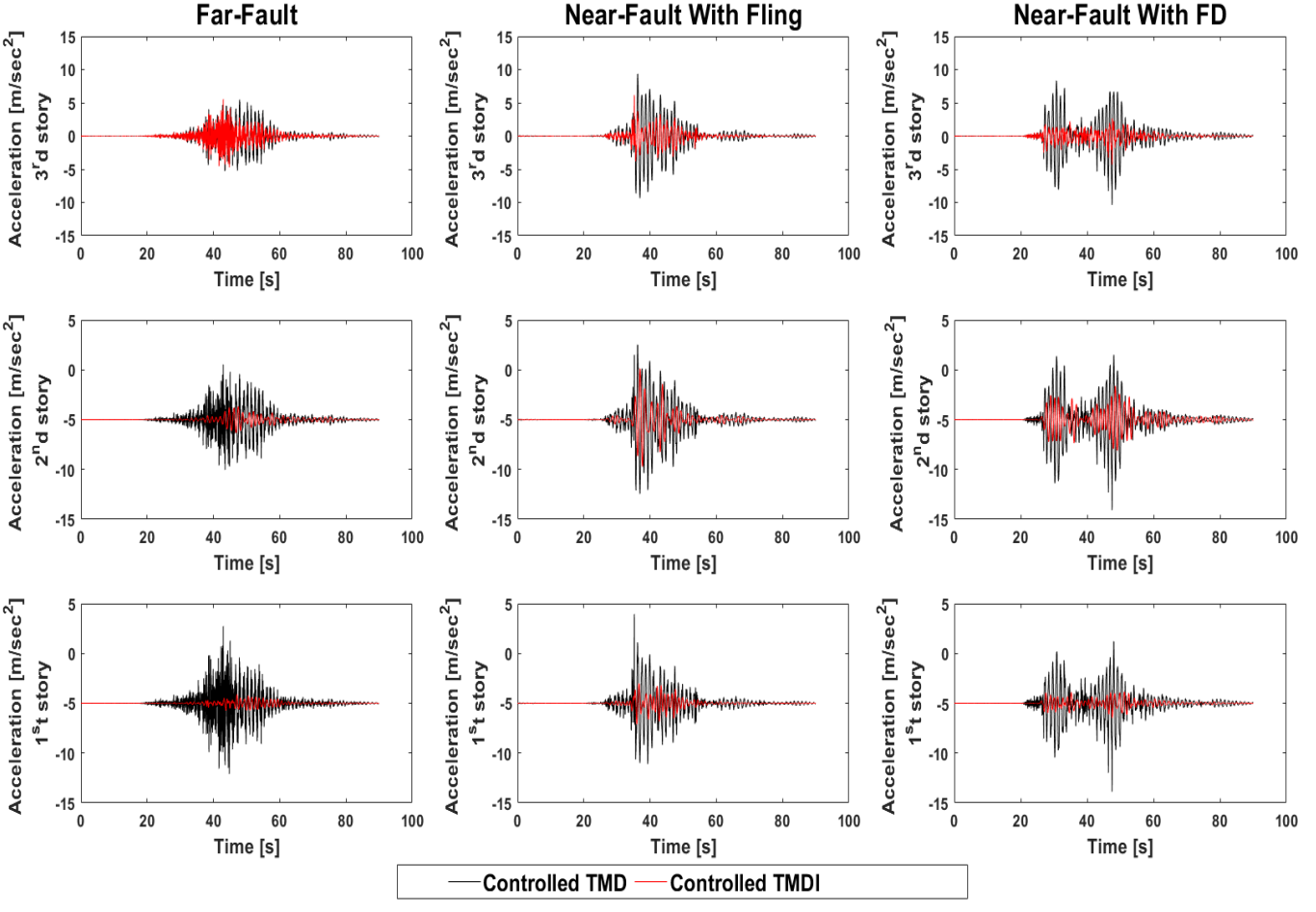

Fig. 7 Induced acceleration time-histories of MDOF structure under the Chi-Chi, Far-Fault, Near-Fault with FD and Near-Fault with fling records, design parameters derived from J_{obj1}.

Table 4. Peak acceleration response quantities at each storey level.

Earthquake	Peak floor acceleration demand [m/s^2]					
	1st storey		2nd storey		3rd storey	
	TMDI	TMD	TMDI	TMD	TMDI	TMD
Chi-Chi far-Fault	0.6312	5.4190	2.3246	5.5368	5.5376	5.4761
Chi-Chi near-fault with FS	1.4698	6.2547	5.1176	7.5376	6.1491	9.3641
Chi-Chi near-fault with FD	1.0282	6.2091	3.3645	9.0844	4.2921	10.3691

Taking into account varying inertance ratios, Fig. 8 depicts the peak response reduction factor ($\boldsymbol{\upsilon}$) against the μs of the building model. The RF values are used to evaluate the effectiveness of TMDs and TMDIs once they have been optimized, which can be defined as:

$$RF = \left(\frac{\max(n^{th}DOF\ uncontrolled\ response) - \max(n^{th}DOF\ controlled\ response)}{\max(n^{th}DOF\ uncontrolled\ response)}\right) * 100 \quad (23)$$

The values of the RF attained with conventional TMD for different μs, 2%, 3%, 5%, and 10%, under far-field records are 21%, 27%, 42%, and 54%, respectively. The aforementioned percentages, in order, are 14%, 22%, 25%, and 34% for the same structure when subjected to near-fault ground motion with FS. Using the Chi-Chi near-fault ground motion with FD, the percentage values achieved are 20%, 25%, 44%, and 50%, respectively. It is possible to deduce, on the basis of these findings, that the $\boldsymbol{\upsilon}$ obviously increases considerably with increasing TMD mass, and that as a result, a greater TMD mass controls the dynamic response of seismically activated structures more effectively. However, the structural system's overall weight will increase as a result of this. More importantly, it is possible to conclude that the highest performance of TMD may be obtained with far-field records and near-field records with FD, and an acceptable performance with near-field records with FS. It's noteworthy that integrating an inerter into conventional TMD having an μ of less than 5% increases the RF, fluctuating from 22% to 37% for far-fault records, and 9%–25% for near-fault motion with FS, as well as fluctuating from 33% to 36% for near-fault motion with $\boldsymbol{\upsilon}$. Consequently, decreasing μs of conventional TMD are necessary to achieve the best reduction factor, RF,

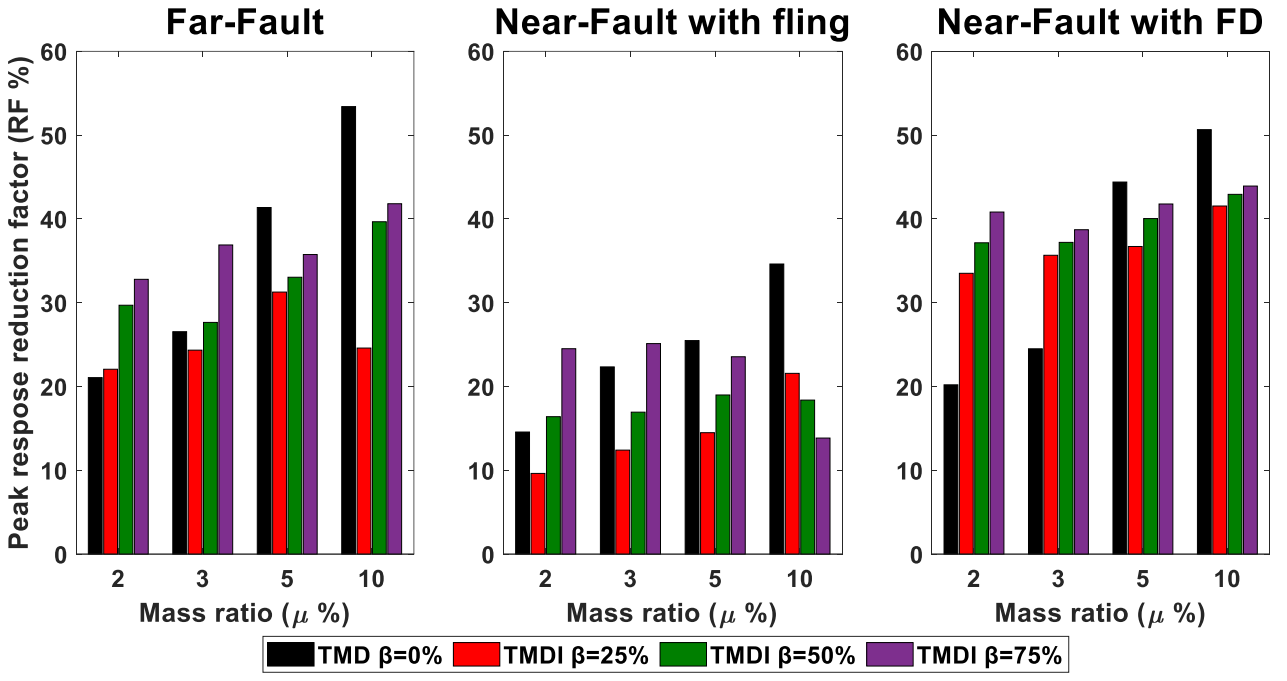

Fig. 8 peak response reduction factor against μs of the building model considering different inertance ratios.

for TMDI-controlled structures. The TMDI-achieved decreases in dynamic response can either retain the behavior of the structure within the elastic range or, in the worst scenario, permit a somewhat nonlinear behavior that could result in repairable structural damage. The trend in the results demonstrates that this effectiveness is mostly attributable to the ground motion's characteristics, which consists of many cycles of pulses with periods that are quite near to the structural period. It would appear that one of the most important factors to consider when determining the efficiency of a control mechanism is the number of inherent pulses of near-fault ground motions that are present.

It is important to take into account the following dimensionless performance index (PI) that was coded in the algorithm. The PI entails comparing the system's uncontrolled response to its controlled response via TMD or TMDI with a focus on the nth degree of freedom. It has been observed that the value of PI has an inverse relation with the amount of improvement that has been achieved.

$$PI = \frac{\max\left(n^{th}DOF\ controlled\ response\right)}{\max\left(n^{th}DOF\ uncontrolled\ response\right)} \quad (24)$$

The results of the peak displacement response quantities and PI obtained for various TMD mass ratios (μ = 1–10% of the main structure's total mass) and three various inertance ratios (β= 25%, 50%, and 75%) compared to the conventional TMD's inertance ratio (β = 0) are shown Fig. 9. The given numerical results clearly demonstrate that the near-fault ground motions with FS produced greater PI values than the far-fault and near-fault with FD ground motions. It is evident for all μs that when the structure is controlled via TMD without the addition of inertance, the decreases in the dynamic response, as measured by the value of PI, are substantially superior. In addition, the performance enhancement is significantly larger for TMD mass values that are greater than 5 % of the primary structure's total mass, whereas it becomes less important for TMD mass values that are less than 3 % of the primary structure's total mass. More crucially, the data show that the inerter device's "mass amplification" effect can be used to effectively substitute some of the TMD's oscillating mass and reduce the structural system's weight while maintaining the primary structure's oscillation below a particular threshold.

As demonstrated in Table 4, under the application of Chi-Chi far-fault ground motions, a perfectly tuned inerter-based device having β = 75% and a TMD mass of 1500 kg produces the same performance level as an optimally tuned conventional TMD with five times higher oscillating mass (7500kg). Also, using Chi-Chi near-fault with FS, a perfectly tuned inerter-based device having β = 75% and a TMD mass of 1500 kg produces the same performance level as an optimally tuned conventional TMD with more than two times heavier oscillating mass (3750kg).

The TMD's stroke is defined as the relative displacement of the TMD in comparison to that of the main structure. The limit on the TMD's strokes is an important consideration in the design of the TMD because it is one of the crucial factors. Fig. 10 shows the stroke amplification factor of the seismically excited controlled building having varied mass ratios ranging from 2% to 10% against the inertance ratio to explore the role of the incorporation of inerter in the TMD configuration in lowering TMD's stroke. The stroke amplification factor is the peak displacement of the attached mass as a function of the inertia, TMDI stroke, divided by the value for a conventional TMD, TMD stroke. As can be seen in the figure, the peak attached mass displacement is drastically reduced when the inerter is incorporated into the TMD configuration.

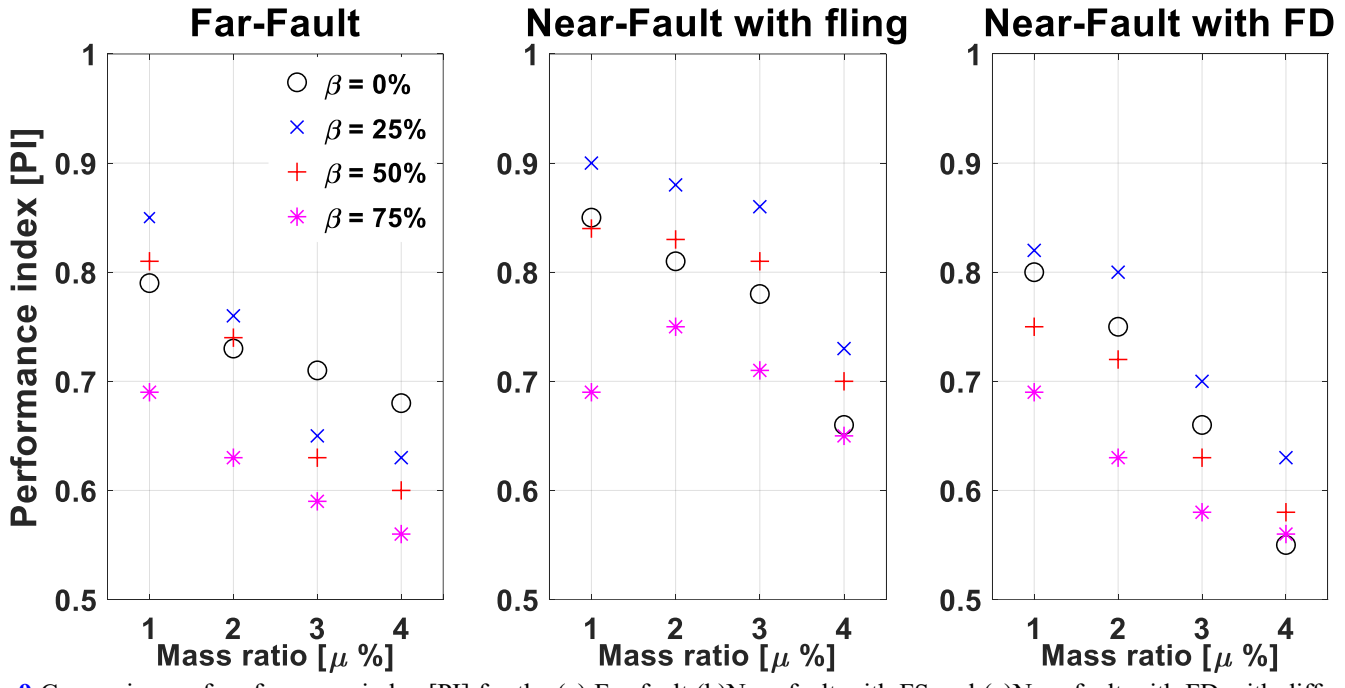

Fig. 9 Comparisons of performance index [PI] for the (a) Far-fault (b)Near-fault with FS and (c)Near-fault with FD with different mass ratios [μ].

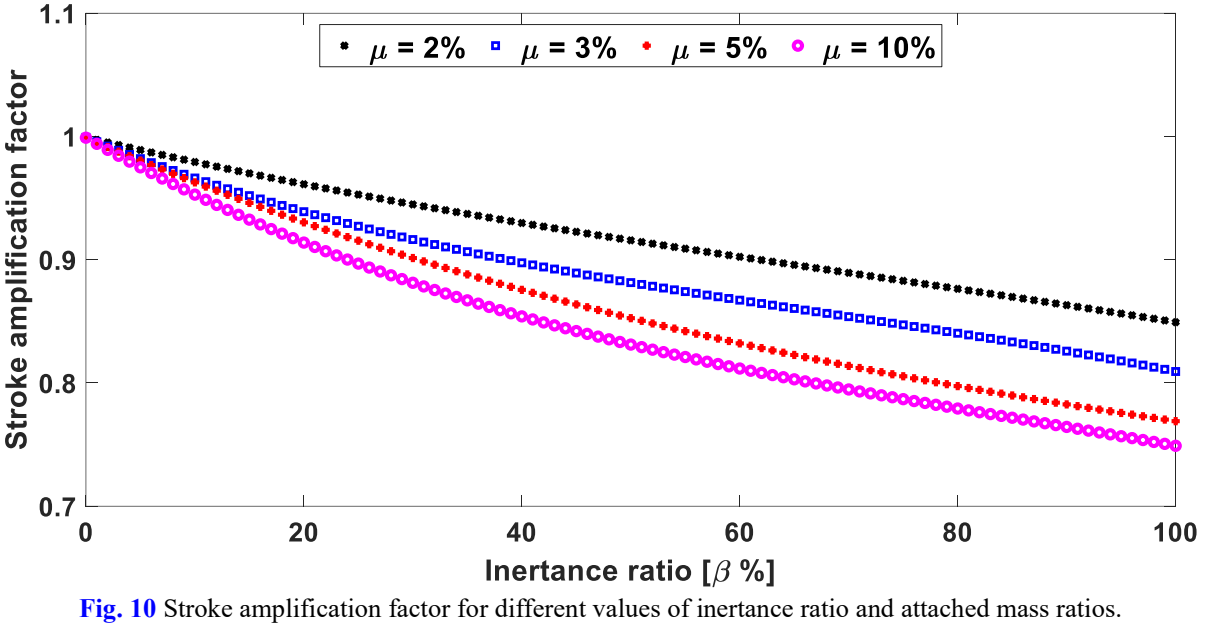

Fig. 10 Stroke amplification factor for different values of inertance ratio and attached mass ratios.

7. Summary and conclusions

Within the scope of this research, an analytical investigation of the impacts of near-fault and far-fault ground motion on the nonlinear dynamic response of controlled structures is carried out. As a result of the forward directivity and fling effect of the near-fault ground motions, the seismic response of structures in the near field of a rupturing fault may differ dramatically from those recorded in the far field. In addition, the impacts of near-fault earthquakes, both those with and without pulses, were not individually assessed for the design of structures in the current version of seismic design codes. Thus, there is a lack of reliable information on their seismic design in the near-fault seismic zone.

This research provides a comprehensive analytical and numerical examination of the possibility of employing tuned mass dampers (TMDs) and tuned mass damper inerters (TMDIs) to control displacement demands on the MDOF building model exposed to far- and near-fault ground motions. The controlled response's bi-objective function minimizes inter-story drifts and horizontal peak floor acceleration separately. In order to take the relevance of the earthquake type into account, three stations have collected data from far- and near-fault locations for the Chi-Chi earthquake that

occurred in 1999. These selected stations correspond, respectively, to far-fault, near-fault with fling step (FS), and near-fault with forward directivity (FD) ground motions. The seismically excited building model studied here was controlled by TMD and TMDI with various configurations of μs (2%, 3%, 5%, and 10%) and inertance ratios (25%, 50%, and 75%). As part of the process of tuning for the appropriate control system parameters ($\boldsymbol{\upsilon}$ and $\boldsymbol{\xi}$), TMD and TMDI are tuned for each ground motion using a genetic algorithm based on near- and far-fault ground motion characteristics. The time-domain differential equation of motion of a damped MDOF primary structure with a TMDI is created in order to achieve the objective of reducing the fundamental mode of vibration. The Laplace transform is used to obtain a closed-form solution for the MDOF lumped-mass structure's equation of motion. As a result of their connections to structural and non-structural component failures, displacement and drift are chosen as performance criteria. These findings provide helpful insights into the effect that the seismology characteristics of ground motion have on the control performance of TMDs and TMDIs and show the necessity of taking the characteristics of ground motion into account while constructing optimal solutions. The following is a summary of the most important conclusions that can be drawn from the findings of the study.

- The TMDI is a popularization of the conventional TMD for exciting building structures. In order to achieve "optimal" performance for the new TMDI configuration, all approaches that have been published in the literature for obtaining optimal design ("tuning") of the conventional TMD are readily applicable. However, ground motion affects the TMDI's optimal tuning frequency.
- Considering the Chi-Chi earthquake, the results of peak response reduction factors (RFs) for TMD devices with mass ratios ranging from 2% to 10% indicate a significant reduction, where decreases in RF values ranging from 14% to 54% have been observed. Consequently, a greater TMD mass controls the dynamic response of the seismically excited structures more effectively. This will result in an increase in the structure's total weight.
- Integrating an inerter into a conventional TMD with an μ of less than 5% increases the RF, ranging from 22% to 37% for far-fault motion and 9% to 25% for near-fault motion with FS and 33% to 36% for near-fault motion with FD. Therefore, it is necessary to reduce the μs of conventional TMD in order to provide the optimal RF for TMDI-controlled structures.
- The trend of the results indicates that ideally designed TMDs are preferable to TMDIs for controlling seismically excited structures, especially those with larger μs and regardless of the nature of the ground motions. Therefore, at larger mass ratios, the addition of inertance to conventional TMDs may have a detrimental influence on the control of seismic responses.
- The ground motions recorded close to the near-fault zones are substantially different from those reported further away from the seismic source, hence it is advised that actual ground motions compatible with the earthquake source mechanism at the site be used to create appropriate control mechanisms. Consequently, the optimum tuning frequency of the TMD and TMDI changes based on the nature of ground motions.
- Near-fault ground motions often catch seismologists' attention because they behave like a pulse. However, it should be noted that they can also have higher frequencies that could negatively influence buildings.
- According to the findings, it is abundantly obvious that the proposed configuration for the TMDI, which incorporates the inerter, is able to accomplish two objectives: mass replacement and mass amplification. The first of these can be accomplished by replacing some of the TMD's oscillating mass to produce a substantially lighter control unit. The second objective can be met by increasing the TMD's performance while maintaining the same TMD mass, which is particularly prominent when the TMD has a small mass. When this is the case, adding the inerter allows viscous dampers with substantially larger damping coefficients than a conventionally tuned TMD.

Further study is required to address issues such as how TMDIs should be optimized for specific civil engineering structures such as base-isolated structures, bridges, dams, and tunnels, take soil flexibility and the effect of the rupture mechanism into account and slip on these structures, and how ground motion uncertainties can be integrated to achieve effective and robust control systems.

Conflict of Interest

There is no conflict of interest.

Supporting Information

Not applicable.

Nomenclature

b	Inertance of the inerter
C	Damping matrix
ci	Damping coefficient of ith degree of freedom
c_{TMDI}	Damper damping coefficient
D_{SS}	Site-source distance
F_{iner}	Inerter's restraining force
g_1	Optimal design parameters vector
hi	Storey height of ith degree of freedom
K	Stiffness matrix
ki	Stiffness of ith degree of freedom
k_{TMDI}	Damper stiffness
M	Mass matrix
M_s	Primary structure's total mass
M_w	Magnitude of earthquake
mi	Mass of ith degree of freedom
m_{TMDI}	Damper mass
T	Natural structural vibration period
$X, \dot{X}, \ddot{X}$	Displacement, velocity and acceleration vectors

$\ddot{x}_g$	Ground acceleration vector
x_i	Horizontal displacement of ith degree of freedom
$\dot{x}_i$	Velocity of ith degree of freedom
$\ddot{x}_i$	Acceleration of ith degree of freedom
x_f	Lateral displacement of floor slab
x_{roof}	Lateral displacement of roof
x_{TMDI}	Lateral displacement of oscillating mass
β	Inertance ratio
ω_i	Natural frequency of ith degree of freedom
ξ	Structural damping ratio
$\boldsymbol{\xi}$	Optimal damper damping ratio
FD	Forward directivity
$\boldsymbol{\upsilon}$	Optimal damper frequency ratio
FS	Fling step
GA	Genetic algorithm
MDOF	Multi degree of freedom
μ	Mass ratio
PGA	Peak ground acceleration
PGV	Peak ground velocity
PI	Performance index
PTMD	particle-tuned mass damper
RF	Response reduction factor
TLD	Tuned liquid damper
TLCD	Tuned liquid column damper
TMD	Tuned mass damper
TMDI	Tuned mass damper inerter

References

[1] I. Avramidis, A. Athanatopoulou, K. Morfidis, A. Sextos, and A. Giaralis, "Eurocode-Compliant Seismic Analysis and Design of R/C Buildings Concepts, Commentary and Worked Examples with Flowcharts, Cham: Springer International Publishing, 2016.

[2] M. D. Symans, F. A. Charney, A. S. Whittaker, M. C. Constantinou, C. A. Kircher, M. W. Johnson, R. J. McNamara, Energy dissipation systems for seismic applications: current practice and recent developments, *Journal of Structural Engineering*, 2008, **134**, 3-21, doi: 10.1061/(asce)0733-9445(2008)134:1(3).

[3] S. Jaisee, F. Yue, Y. H. Ooi, A state-of-the-art review on passive friction dampers and their applications, *Engineering Structures*, 2021, **235**, 112022, doi: 10.1016/j.engstruct.2021.112022.

[4] L. Faravelli, Passive energy dissipation systems in structural engineering by T. T. Soong and G. F. Dargush John Wiley & Sons Chichester, 1997 ISBN 0-471-96821-8, *Journal of Structural Control*, 1999, **6**, 172, doi: 10.1002/stc.4300060114.

[5] G. Dargush, T. Soong, Passive energy dissipation systems in structural engineering, Wiley, New York, 1997.

[6] B. F. Spencer Jr, S. Nagarajaiah, State of the art of structural control, *Journal of Structural Engineering*, 2003, **129**, 845-856, doi: 10.1061/(asce)0733-9445(2003)129: 7(845).

[7] T. T, Soong, Supplemental energy dissipation: state-of-the-art and state-of-the-practice, *Engineering Structures*, 2002, **24**, 243-259, doi: 10.1016/S0141-0296(01)00092-X.

[8] P. Scott, Harvey, Jr, A review of rolling-type seismic isolation: historical development and future directions, *Engineering Structures*, 2016, **125**, 521-531, doi: 10.1016/j.engstruct.2016.07.031.

[9] Y. Bozorgnia, V. V. Bertero (Eds.) Earthquake engineering from engineering seismology to performance-based engineering, *CRC Press*, Boca Raton, 2004, 676-715, doi: 10.1201/9780203486245.

[10] S. Elias, V. Matsagar, Research developments in vibration control of structures using passive tuned mass dampers, *Annual Reviews in Control*, 2017, **44**, 129-156, doi: 10.1016/j.arcontrol.2017.09.015.

[11] J. P. Den Hartog, Mechanical Vibrations, New York, McGraw-Hill, NY, 1956.

[12] Ayman, Abd-Elhamed, Simulation analysis of TMD controlled building subjected to far- and near-fault records considering soil-structure interaction, *Journal of Building Engineering*, 2019, **26**, 100930, doi: 10.1016/j.jobe.2019.100930.

[13] D. K. Pandey, M. K. Sharma, S. K. Mishra, A compliant tuned liquid damper for controlling seismic vibration of short period structures, *Mechanical Systems and Signal Processing*, 2019, **132**, 405-428, doi: 10.1016/j.ymssp.2019.07.002.

[14] A. Pabarja, M. Vafaei, S. C. Alih, M. Y. Md Yatim, S. A. Osman, Experimental study on the efficiency of tuned liquid dampers for vibration mitigation of a vertically irregular structure, *Mechanical Systems and Signal Processing*, 2019, **114**, 84-105, doi: 10.1016/j.ymssp.2018.05.008.

[15] Ayman, Abd-Elhamed, Tuned liquid damper for vibration mitigation of seismic-excited structures on soft soil, *Alexandria Engineering Journal*, 2022, **61**, 9583-9599, doi: 10.1016/j.aej.2022.03.051.

[16] M. J. Hochrainer, F. Ziegler, Control of tall building vibrations by sealed tuned liquid column dampers, *Structural Control and Health Monitoring*, 2006, **13**, 980-1002, doi: 10.1002/stc.90.

[17] J. S. Love, M. J. Tait, H. Toopchi-Nezhad, A hybrid structural control system using a tuned liquid damper to reduce the wind induced motion of a base isolated structure, *Engineering Structures*, 2011, **33**, 738-746, doi: 10.1016/j.engstruct.2010.11.027.

[18] A. Matteo, T. Furtmüller, C. Adam, A. Pirrotta, Optimal design of tuned liquid column dampers for seismic response control of base-isolated structures, *Acta Mechanica*, 2018, **229**, 437-454, doi: 10.1007/s00707-017-1980-7.

[19] E. Matta, Performance of tuned mass dampers against near-field earthquakes, *Structural Engineering and Mechanics*, 2011, **39**, 621-642, doi: 10.12989/sem.2011.39.5.621.

[20] Q. Wang, H.-N. Li, P. Zhang, Vibration control of a high-rise slender structure with a spring pendulum pounding tuned mass damper, *Actuators*, 2021, **10**, 44, doi: 10.3390/act10030044.

[21] S. Elias, V. Matsagar, Research developments in vibration control of structures using passive tuned mass dampers, *Annual Reviews in Control*, 2017, **44**, 129-156, doi: 10.1016/j.arcontrol.2017.09.015.

[22] C. Sun, Mitigation of offshore wind turbine responses under wind and wave loading: considering soil effects and damage, *Structural Control and Health Monitoring*, 2018, **25**, e2117, doi: 10.1002/stc.2117.
[23] A. Bathaei, S. M. Zahrai, M. Ramezani, Semi-active seismic control of an 11-DOF building model with TMD+MR damper using type-1 and-2 fuzzy algorithms, *Journal of Vibration and Control*, 2018, **24**, 2938-2953, doi: 10.1177/1077546317696369.
[24] P. Lieber, D. P. Jensen, An acceleration damper: development, design, and some applications, *Journal of Fluids Engineering*, 1945, **67**, 523-530, doi: 10.1115/1.4018316.
[25] Z. Lu, X. Chen, D. Zhang, K. Dai, Experimental and analytical study on the performance of particle tuned mass dampers under seismic excitation, *Earthquake Engineering & Structural Dynamics*, 2017, **46**, 697-714, doi: 10.1002/eqe.2826.
[26] Zheng, Lu, An equivalent method for optimization of particle tuned mass damper based on experimental parametric study, *Journal of Sound and Vibration*, 2018, **419**, 571-584, doi: 10.1016/j.jsv.2017.05.048.
[27] Z. Lu, K. Li, Y. Ouyang, J. Shan, Performance-based optimal design of tuned impact damper for seismically excited nonlinear building, *Engineering Structures*, 2018, **160**, 314-327, doi: 10.1016/j.engstruct.2018.01.042.
[28] Z. Lu, C. Zhou, K. Rong, J. Zhang, J. Du, Vibration reduction mechanism of a novel enhanced particle inerter device, *International Journal of Structural Stability and Dynamics*, 2023, **23**, 2350009, doi: 10.1142/s0219455423500098.
[29] F. Weber, P. Huber, F. Borchsenius, C. Braun, Performance of TMDI for tall building damping, *Actuators*, 2020, **9**, 139, doi: 10.3390/act9040139.
[30] A. Di Matteo, C. Masnata, A. Pirrotta, Simplified analytical solution for the optimal design of Tuned Mass Damper Inerter for base isolated structures, *Mechanical Systems and Signal Processing*, 2019, **134**, 106337, doi: 10.1016/j.ymssp.2019.106337.
[31] D. De Domenico, P. Deastra, G. Ricciardi, N. D. Sims, D. J. Wagg, Novel fluid inerter based tuned mass dampers for optimised structural control of base-isolated buildings, *Journal of the Franklin Institute*, 2019, **356**, 7626-7649, doi: 10.1016/j.jfranklin.2018.11.012.
[32] A. Giaralis, A. A. Taflanidis, Optimal tuned mass-damper-inerter (TMDI) design for seismically excited MDOF structures with model uncertainties based on reliability criteria, *Structural Control and Health Monitoring*, 2018, **25**, e2082, doi: 10.1002/stc.2082.
[33] R. Ruiz, A. A. Taflanidis, A. Giaralis, D. Lopez-Garcia, Risk-informed optimization of the tuned mass-damper-inerter (TMDI) for the seismic protection of multi-storey building structures, *Engineering Structures*, 2018, **177**, 836-850, doi: 10.1016/j.engstruct.2018.08.074.
[34] D. De Domenico, H. Qiao, Q. Wang, Z. Zhu, G. Marano, Optimal design and seismic performance of Multi-Tuned Mass Damper Inerter (MTMDI) applied to adjacent high-rise buildings, *The Structural Design of Tall and Special Buildings*, 2020, **29**, e1781, doi: 10.1002/tal.1781.
[35] F. Palacios-Quiñonero, J. Rubió-Massegú, J. M. Rossell, H. R. Karimi, Design of inerter-based multi-actuator systems for vibration control of adjacent structures, *Journal of the Franklin Institute*, 2019, **356**, 7785-7809, doi: 10.1016/j.jfranklin.2019.03.010.
[36] A. R. Özuygur, E. Noroozinejad Farsangi, Influence of pulse-like near-fault ground motions on the base-isolated buildings with LRB devices, *Practice Periodical on Structural Design and Construction*, 2021, **26**, 04021027, doi: 10.1061/(asce)sc.1943-5576.0000603.
[37] R. Whitney, Synthetic pulse model for near-fault effects on structures, *Practice Periodical on Structural Design and Construction*, 2020, **25**, 04020013, doi: 10.1061/(asce)sc.1943-5576.0000490.
[38] M. Jami, S. Elias, R. Rupakhety, D. De Domenico, G. Falsone, G. Ricciardi, Are bridges safe under near-fault pulse-type ground motions considering the vertical component? Lecture Notes in Civil Engineering. Cham: Springer International Publishing, 2021: 1207-1215, doi: 10.1007/978-3-030-91877-4_137.
[39] G. P. Mavroeidis, A. S. Papageorgiou, A mathematical representation of near-fault ground motions, *Bulletin of the Seismological Society of America*, 2003, **93**, 1099-1131, doi: 10.1785/0120020100.
[40] R. Rupakhety, S. U. Sigurdsson, A. S. Papageorgiou, R. Sigbjörnsson, Quantification of ground-motion parameters and response spectra in the near-fault region, *Bulletin of Earthquake Engineering*, 2011, **9**, 893-930, doi: 10.1007/s10518-011-9255-5.
[41] T. Saito, Response of high-rise buildings under long period earthquake ground motions, *International Journal of Structural and Civil Engineering Research*, 2016, **5**, 308-14, doi: 10.18178/ijscer.5.4.308-314.
[42] P. G. Somerville, Magnitude scaling of the near fault rupture directivity pulse, *Physics of the Earth and Planetary Interiors*, 2003, **137**, 201-212, doi: 10.1016/S0031-9201(03)00015-3.
[43] D. Jonathan, Bray, Characterization of forward-directivity ground motions in the near-fault region, *Soil Dynamics and Earthquake Engineering*, 2004, **24**, 815-828, doi: 10.1016/j.soildyn.2004.05.001.
[44] G. Ö. Sigurðsson, R. Rupakhety, S. E. Rahimi, S. Olafsson, Effect of pulse-like near-fault ground motions on utility-scale land-based wind turbines, *Bulletin of Earthquake Engineering*, 2020, **18**, 953-968, doi: 10.1007/s10518-019-00743-9.
[45] F. Mazza, A. Vulcano, Effects of near-fault ground motions on the nonlinear dynamic response of base-isolated r.c. framed buildings, *Earthquake Engineering & Structural Dynamics*, 2012, **41**, 211-232, doi: 10.1002/eqe.1126.
[46] T. Yang, Y. Wei, J. Zhong, Potential bias of conventional structural seismic fragility for bridge structures under pulse-like ground motions: bias evaluation and strategy improvement, *Soil Dynamics and Earthquake Engineering*, 2023, **166**, 107787, doi: 10.1016/j.soildyn.2023.107787.
[47] T. Yang, X. Yuan, J. Zhong, W. Yuan, Near-fault pulse seismic ductility spectra for bridge columns based on machine

learning, *Soil Dynamics and Earthquake Engineering*, 2023, **164**, 107582, doi: 10.1016/j.soildyn.2022.107582.
[48] Jian, Zhong, Uncoupled multivariate power models for estimating performance-based seismic damage states of column curvature ductility, *Structures*, 2022, **36**, 752-764, doi: 10.1016/j.istruc.2021.12.041.
[49] J. Zhong, T. Yang, Y. Pang, W. Yuan, A novel structure-pulse coupled model for quantifying the column ductility demand under pulse-like GMs, *Journal of Earthquake Engineering*, 2022, **26**, 8185-8203, doi: 10.1080/13632469.2021.1989348.
[50] J. Salvi, E. Rizzi, E. Rustighi, N. S. Ferguson, Optimum tuning of passive tuned mass dampers for the mitigation of pulse-like responses, *Journal of Vibration and Acoustics*, 2018, **140**, 061014, doi: 10.1115/1.4040475.
[51] M. Domizio, D. Ambrosini, O. Curadelli, Performance of TMDs on nonlinear structures subjected to near-fault earthquakes, *Smart Structures and Systems*, 2015, **16**, 725-742, doi: 10.12989/sss.2015.16.4.725.
[52] E. Barredo, J. G. Mendoza Larios, J. Mayén, A. A. Flores-Hernández, J. Colín, M. Arias Montiel, Optimal design for high-performance passive dynamic vibration absorbers under random vibration, *Engineering Structures*, 2019, **195**, 469-489, doi: 10.1016/j.engstruct.2019.05.105.
[53] E. Barredo, J. G. Mendoza Larios, J. Colín, J. Mayén, A. A. Flores-Hernández, M. Arias-Montiel, A novel high-performance passive non-traditional inerter-based dynamic vibration absorber, *Journal of Sound and Vibration*, 2020, **485**, 115583, doi: 10.1016/j.jsv.2020.115583.
[54] A. Abd-Elhamed, M. Fathy, K. M. Abdelgaber, Closed-form solutions of dynamic vibration equations of seismically excited structures, *Arab Journal of Basic and Applied Sciences*, 2022, **29**, 318-329, doi: 10.1080/25765299.2022.2124754.
[55] A. Abd-Elhamed, S. Mahmoud, Seismic response evaluation of structures on improved liquefiable soil, *European Journal of Environmental and Civil Engineering*, 2021, **25**, 1695-1717, doi: 10.1080/19648189.2019.1595738.
[56] S. Mahmoud, A. Abd-Elhameed, R. Jankowski, Behaviour of colliding multi-storey buildings under earthquake excitation considering soil-structure interaction, *Applied Mechanics and Materials*, 2012, **166-169**, 2283-2292, doi: 10.4028/www.scientific.net/amm.166-169.2283.
[57] A. Abd-Elhamed, S. Alkhatib, A. M. H. Abdelfattah, Prediction of blast-induced structural response and associated damage using machine learning, *Buildings*, 2022, **12**, 2093, doi: 10.3390/buildings12122093.